Chemical Engineering Journal 166 (2011) 256–268

Contents lists available at ScienceDirect

Chemical Engineering Journal

journal homepage: www.elsevier.com/locate/cej

Reverse electrodialysis: A validated process model for design and optimization

J. Veerman[a,b], M. Saakes[a], S.J. Metz[a,*], G.J. Harmsen[c]

[a] Wetsus, Centre of Excellence for Sustainable Water Technology, P.O. Box 1113, 8900 CC Leeuwarden, The Netherlands
[b] NHL Hogeschool, Department of Life Sciences and Technology, Agora 1, 8934 CJ Leeuwarden, The Netherlands
[c] University of Groningen, Nijenborgh 4, 9747 AG Groningen, The Netherlands

ARTICLE INFO

Article history:
Received 18 May 2010
Received in revised form 25 October 2010
Accepted 27 October 2010

Keywords:
Reverse electrodialysis
Electrodialysis
Salinity gradient power
Renewable energy
Power production

ABSTRACT

Reverse electrodialysis (RED) is a technology to generate electricity using the entropy of the mixing of sea and river water. A model is made of the RED process and validated experimentally. The model is used to design and optimize the RED process. It predicts very small differences between counter- and co-current operation.

It was decided to focus on co-current design because co-current operation causes smaller local pressure differences between the river and seawater compartments—hence smaller risk of leakages and the possibility to use very thin membranes with high fluxes and very open spacer structures with low hydrodynamic resistance.

Segmentation of the electrodes proved to increase the power density by about 15% under realistic operational conditions. The model shows that with smaller systems – in terms of length of the flow path – higher power densities are possible. This effect is rather dramatical and poses a challenge for designing improved RED stacks on large commercial scale. It is suggested to reduce the flow path length by applying a fractal structure design of the spacers. Such structures can be made by profiling the membrane.

1. Introduction

New renewable forms of energy are needed without thermal pollution, without emission of environmental unwanted substances and without net emission of greenhouse gasses. Wind power, hydropower, biofuel, solar power, geothermal power and ocean power are contributors to an economy of renewable energy. A relative young member of this group is salinity gradient power (SGP), the energy that can be generated from reversible mixing of two kinds of water with different salt contents. This technique is proposed by Pattle in 1954 [1,2].

The global potential of SGP is the product of the potential energy density of river water times the flow rate of all river water in the world. Notwithstanding the local variations in salinity and temperature of the sea and river water, the average value of the energy content of river water can be used for an estimation of the global power. This energy content is about 2.5×10^6 J/m^3, supposing that a large excess of seawater is used. The total discharge of all rivers in the world is estimated to be 1.13×10^6 m^3/s [3]. Therefore, the global potential power is 2.8 TW, a value near to the 2.6 TW as estimated in 1977 by Wick and Schmitt [4]. In 2008, the average world energy consumption was about 15 TW; 5 TW from this amount was used to generate 2 TW of electrical energy in most low efficient coal fired power plants [5]. Thus the potential of SGP is more than the current global electricity consumption.

The advantages of SGP are: limitless supply (if river and the seawater is used), no production of pollutants like NO_x, no CO_2-exhaust, no thermal pollution, no radioactive waste and no daily fluctuations in the productions due to variations in wind speed or sunshine. However, in relation to other fuels, the salinity gradient energy content of river water is rather poor. Consequently, investment costs for a SGP plan may be rather high and transportation costs of feed water to the plant and inside the plant is substantial.

There are two membrane-based technologies which can convert this potential energy into useful electricity: reverse electrodialysis (RED) and pressure retarded osmosis (PRO). It has been shown that, in the case of river water with seawater, RED is a promising technique [6].

An important performance parameter is the power density. In 1980, Lacey presented a model of RED and calculated theoretical power densities [7] while defining power density as power per membrane pair area. Weinstein and Leitz [8] also used the membrane pair area in that respect. Such approach is conform to electrochemical research practice. However, there is no real consensus in literature since e.g. Jagur-Grodzinsky and Kramer used the total membrane area [9]. When the Blue Energy project was started in 2005 at the Wetsus institute in the Netherlands, a first aim within that project was to compare the performance of RED

* Corresponding author. Tel.: +31 58 2843 000.
E-mail address: sybrand.metz@wetsus.nl (S.J. Metz).

1385-8947/$ – see front matter © 2010 Elsevier B.V. All rights reserved.
doi:10.1016/j.cej.2010.10.071

Nomenclature

A	cell area (m^2)
A_m	total membrane area (m^2)
A_{Na^+}	effective hydrated ion radius of Na^+ (pm)
A_{Cl^-}	effective hydrated ion radius of Cl^+ (pm)
b	width of a cell (m)
C	concentration (mol/m^3)
D_{salt}	diffusion constant of NaCl (m^2/s)
D_{water}	diffusion constant of water (m^2/s)
D	hydraulic diameter (m)
E	voltage (V)
E_{cell}	electromotive force of one cell (V)
F	Faraday constant (96,485 C/mol)
f	obstruction factor
I	ion strength of a solution (mol/L)
i	electrical current (A)
j	current density (A/m^2)
J_{NaCl}	flux of NaCl ($mol\,s^{-1}\,m^{-2}$)
J_{Na}, J_{Cl}	flux of Na^+, Cl^- ($mol\,s^{-1}\,m^{-2}$)
J_{water}	molar flux of water ($mol\,s^{-1}\,m^{-2}$)
J'_{water}	volumetric flux of water (m/s)
L	length of a cell (m)
M_{NaCl}	mass NaCl (0.05844 kg/mol)
M_{H_2O}	mol mass H_2O (0.01802 kg/mol)
N	number of cells in a stack
n_e	degree of segmentation of electrodes
OCV	open circuit voltage (V)
P	power (W)
P_d	power density (W/m^2)
P_{d-net}	net power density (W/m^2)
P_{hydr}	hydraulic power loss (W)
P_i	internal dissipated power (W)
P_{net}	net produced power (W)
P_u	produced electrical power (W)
ΔP	pressure drop (Pa)
Q	pressure drop factor
R	gas constant ($8.314\,J\,mol^{-1}\,K^{-1}$)
R_a	area resistance (Ωm^2)
R_{AEM}	area resistance of the AEM (Ωm^2)
R_{CEM}	area resistance of the CEM (Ωm^2)
R_{cell}	cell resistance (Ω)
R_u	external resistance (Ω)
$R_P{}^Z$	response product ($J^2\,m^5\,s^{-1}$)
Re	Reynolds number
S	salt content (kg/m^3)
T	temperature (K)
t_R	residence time (s)
U	voltage (V)
v	average velocity (m/s)
x	flow path direction (m)
X^i	exergy flow rate of the inlet (W)
X^o	exergy flow rate of the effluent (W)
Z_{net}	net river water yield (J/m^3)
z	valency of an ion

Greek symbols

α	permselectivity of the ion exchange membrane
γ	activity coefficient
δ_m	membrane thickness (m)
δ_R	river water compartment thickness (m)
δ_S	seawater compartment thickness (m)
δ_m	membrane thickness (m)
η_T	thermodynamic efficiency
Λ_m	molar conductivity ($S\,m^2/mol$)
ρ_{H_2O}	density of water ($1000\,kg/m^3$)
μ	dynamic viscosity (Pa s)
Φ	flow rate (m^3/s)

Superscripts

i	in
o	out

Subscripts

cit	co-ion transport
coul	coulombic
M	equilibrium
osm	osmotic
R	river
S	sea

Abbreviations

AEM	anion exchange membrane
CEM	cation exchange membrane
ED	electrodialysis
OCV	open circuit voltage
RED	reverse electrodialysis
SGP	salinity gradient power

Definitions

compartment	space between the membranes
cell	combination of two membranes and two compartments
electrode system	the anode, cathode and electrode rinse
stack	a number of N cells with an electrode system
α-mode	a system optimized for maximal net power density (P_{d-net})
β-mode	a system optimized for maximal response product ($R_P{}^Z = Z_{net}P_{d-net}$)

with PRO and, as a result, it was then preferred to use the total membrane area [6].

At that time, the history of RED from river and seawater was limited. Pattle reported the first RED experiments [1,2] and achieved a power density (power per square meter membrane) of 0.05 W/m^2. Weinstein and Leitz achieved 0.17 W/m^2 [8], Audinos 0.40 W/m^2 [10,11], Jagur-Grodzinski and Kramer 0.41 W/m^2 [9], Turek and Bandura 0.46 W/m^2 [12], and Suda et al. 0.26 W/m^2 [13].

Besides power density, the efficiency of the process is an important item. From these pioneers of RED, only Audinos reported the yield (7–22%), however, with brine feed water instead of seawater. From the Wetsus institute, Post et al. showed that with a recirculating feed, very high efficiencies (>80%) are possible at a low current density [14]. However, practical values – at conditions of maximum power density – of the efficiency proved to be much lower (18%) [15].

Our obtained power density was 0.95–1.18 W/m^2 in small stacks of 10 cm × 10 cm [16,17] but substantial lower in larger stacks of 25 cm × 75 cm [17]. For further scale-up the RED process, a model is necessary, describing the RED process and forecasting the power density and efficiency. With such a model, spacer thicknesses and flow rates can be optimized.

To clarify the subject of investigation in this paper, first we will describe all essential elements. Fig. 1 shows a RED stack, consisting (from left to right) of an anode, a number of alternately stacked anion exchange membranes (AEM) and cation exchange membranes (CEM), and a cathode. The compartments between the

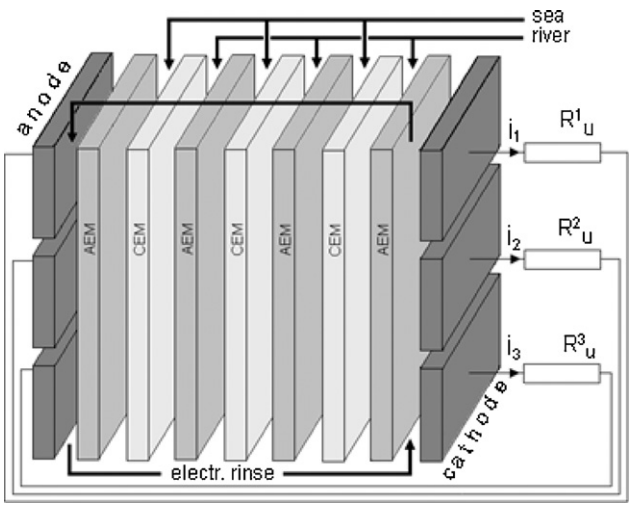

Fig. 1. A RED stack with electrodes divided into three segments and three loads ($R^1{}_u$, $R^2{}_u$ and $R^3{}_u$).

membranes are fed with sea and river water; the compartments between electrodes and outer membranes contain the electrode rinse solution which is circulated through anode and cathode compartments. The cells – consisting of an AEM, a seawater compartment, a CEM and a river water compartment – are the repeating units in a stack; the number of cells (N) may be small in a test setup or large (hundreds up to thousands) in a real economically operating stack. Cations from the seawater diffuse through the CEMs to the river water compartment and build up a positive potential on the cathode. The anions from the seawater diffuse through the AEMs to the river water compartment on the other side and cause a negative potential on the anode. Electrical power can be extracted from the system by an external circuit connected to the electrodes. The ionic current within the cells is then converted to an external electron current via redox reactions at the electrodes. These electrodes can be undivided or divided into some segments (i.e. in three segments as shown in Fig. 1). With the undivided electrodes, there is only one load (i.e. an external resistance) R_u; in the system with the segmented electrodes, each electrode has its own load.

In this paper we describe a process model containing all key elements of hydrodynamics, membrane transport and the electrode system. This model is first validated with the experimental data of our various test facilities for all key parameters and then it is used to design and optimize the RED process.

2. Process model description

2.1. Energy balance and response variables

The feed water entering a RED stack represents a certain amount of exergy X^i [18,19]:

$$X^i = 2RT\left[\Phi_R C_R \ln\frac{C_R}{C_M} + \Phi_S C_S \ln\frac{C_S}{C_M}\right] \quad (1)$$

where X^i is the exergy flow rate of the feed, R is the gas constant (8.314 J mol^{-1} K^{-1}), T temperature (K), Φ_R and Φ_S flow rates of river and seawater (m^3/s) and C_R and Cs the salt concentrations in the river and seawater (mol/m^3). C_M is the equilibrium concentration, obtained at total mixing of river and seawater:

$$C_M = \frac{\Phi_R C_R + \Phi_S C_S}{\Phi_R + \Phi_S} \quad (2)$$

Analogous to Eqs. (1) and (2) – using the outlet concentrations and outlet temperature – the outgoing (X^o) exergy flow rate is achieved from the outlet concentrations of the RED stack. Even in the case of a total conversion, the temperature decrease is only a fraction of a degree. Therefore, we shall use T for inlet as for outlet temperature.

The produced electrical power of the stack (P_u) is the product of the voltage (U) over an external resistor and the current (i) through that resistor:

$$P_u = Ui \quad (3)$$

The produced power is related to the exergy decrease. The efficiency of the process is expressed by the thermodynamic efficiency η_T. In the ideal case the mixing is totally reversible ($\eta_T = 1$) and in the worst case the mixing is total irreversible ($\eta_T = 0$).

$$\eta_T = \frac{P_u}{X^i - X^o} \quad (4)$$

Under conditions of maximal power, the thermodynamic efficiency is only 50% or less [20].

In a RED stack, there are three key response parameters. The first is the net produced power P_{net}, being the produced electrical power P_u minus the hydrodynamic loss P_{hydr}:

$$P_{net} = P_u - P_{hydr} \quad (5)$$

P_{hydr} is the product of the pressure drop over the stack (ΔP_S and ΔP_R for the sea and river water compartment) and the flow rate (Φ_S and Φ_R) for the two feeds:

$$P_{hydr} = \Delta P_S \Phi_S + \Delta P_R \Phi_R \quad (6)$$

The second important response parameter is the power density P_d, the produced electrical power divided by the total membrane area A_m. For the net power density P_{d-net}, this value is corrected for the hydrodynamic loss:

$$P_d = \frac{P_u}{A_m} \quad (7)$$

$$P_{d-net} = \frac{P_{net}}{A_m} \quad (8)$$

Power density is an important parameter, because the membrane area is related to the total investment costs of a RED power plant.

From the starting point that the availability of river water is the limiting factor, it is useful to define an efficiency measure directly from the consumed amount of river water. We call it 'net river water yield' (Z_{net}).

$$Z_{net} = \frac{P_{net}}{\Phi_R} \quad (9)$$

Maximization of Z_{net} may result to unpractical values also: very long residence times in combination with low power densities. Therefore, we introduce the response product $R_P{}^Z$:

$$R_P{}^Z = P_{d-net} Z_{net} \quad (10)$$

2.2. Overview of the modeling of mass and charge transport; equivalent electrical circuits of systems with undivided and with segmented electrodes

In order to simulate the performance of a RED stack, the transport of counter-ions through the membranes should be calculated: Na^+ through the CEMs and Cl^- through the AEMs from the seawater into the river water compartments. Two disturbing effects should taken into account: co-ion transport (Na^+ through the AEMs and Cl^- through the CEMs) in the same direction and osmosis (H_2O transport from the river water to the seawater compartments). Of special interest are the influence of the flow direction (co-current or counter-current) and the degree of segmentation of the electrodes

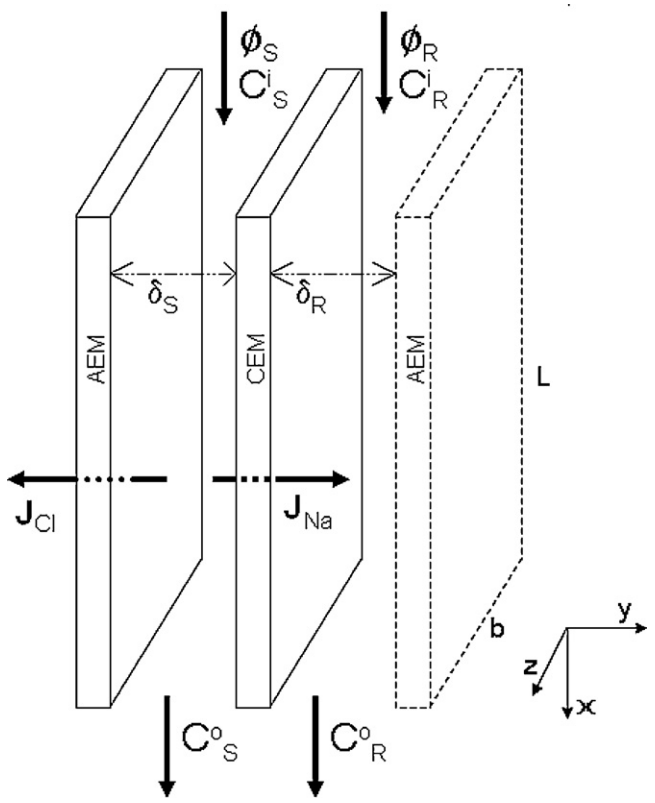

Fig. 2. One cell in a RED stack. The solid part is the repeating unit; the dashed membrane is part of the adjacent cell.

($n_e = 1$: undivided or $n_e > 1$: segmented). We will focus on a single RED cell; effects of parasitic currents – as can be found in stacks with more cells – are not included in this model but were object of a former study [20]. This and the following sections will describe the system and the equations used to define the model and derive the properties of the model.

Fig. 2 shows a single RED cell, consisting (from left to right) of an AEM, a seawater compartment, a CEM and a river water compartment. In the picture the AEM of the adjacent cell is drawn with dashed lines. The dimensions of the stack are described by length (L), width (b), thickness of seawater compartment (δ_S) and thickness of the river water compartment (δ_R). Flow rates of sea and river water are designated by Φ_S and Φ_R and input concentrations by C^i_S and C^i_R.

The cell of Fig. 2 is operated in co-current mode; near the feed water inlets, the electrical resistance is determined by the resistance of the river water compartment (the resistance of the river water is much higher than of the seawater). During the passage of the feed water through the cell, the salt concentration of the seawater decreases and of the river water increases. The consequences are (in the direction of the flow) a decreasing electrical cell resistance and a decreasing voltage. In most test stacks, all parts of the stack share the same electrodes ($n_e = 1$). This situation is not optimal because for maximal power the resistance of the load should be equal to the internal resistance. In the worst case it is imaginable that the upper part of the cell generates power, the middle part does nothing and the lower part acts in the reverse direction (like a normal electrodialysis (ED) unit).

In principle, the stack can be improved by electrode segmentation. In Fig. 1, the electrode is divided into three parts ($n_e = 3$), each with its own load (R_u). Maximal power is generated if each load R_u equals the internal resistance R_{cell} of a specific part of the RED cell [20]. Theoretically, the more the electrode is segmented, the higher the efficiency. In the following sections, a model is developed for both extreme cases: systems with unsegmented electrodes and systems with indefinitely segmented electrodes. The equivalent electrical circuits of systems with undivided and with segmented electrodes are shown in Fig. 3a and b.

2.3. Modeling of the salt and charge transport in a system with infinite segmented electrodes

Electrodes can be undivided as in Fig. 3a or segmented into three parts as in Figs. 1 and 3b or segmented to another degree (n_e). First we will present the theory for a system with an infinite degree of segmentation ($n_e = \infty$), each segment with its own external load. This gives a simple continuous model by which several effects of design variables on the response variables can be studied. The system of differential equations is programmed in *Berkeley Madonna*. This program can be adapted to an undivided electrode system ($n_e = 1$). The extreme values of the segmentation number ($n_e = 1$ and ∞) are sufficient for general conclusions concerning segmentation. In Section 5.3 the effect of intermediate values of the segmentation number ($n_e = 1 \ldots 7$) on the power density is discussed.

In the first order approximation, it is assumed that the salt concentration in the compartments of the cell is uniform in the direction perpendicular to the membranes. This is the well-known plug flow reactor (PFR) approach. However, boundary layers (enrichment or depletion layers) can affect the performance of a RED stack, as showed by Lacey [7] and Długołęcki et al. [21–23]. Transport of salt from sea to river is caused by diffusion of Na^+-ions through the CEM and of Cl^--ions through the AEM. In real membranes there is also a small co-ion transport.

We describe the performance of the RED cell with the following system of 11 equations. The first of this system (Eq. (11)) is the expression of the electromotive force of the cell (E_{cell}). This voltage is the sum of the Nernst potential difference over the CEM and over the AEM [20].

$$E_{cell}(x) = \alpha_{CEM}\frac{RT}{F}\ln\frac{\gamma_S^{Na}(x)C_S(x)}{\gamma_R^{Na}(x)C_R(x)} + \alpha_{AEM}\frac{RT}{F}\ln\frac{\gamma_S^{Cl}(x)C_S(x)}{\gamma_R^{Cl}(x)C_R(x)} \quad (11)$$

In this expression, R is the gas constant (8.314 J mol^{-1} K^{-1}), T is the temperature and F is the Faraday number (96,485 C/mol); α is the permselectivity of the membrane, a measure for the specificity of the membrane for the permeability of counter-ions. Concentrations (in mol/m^3) are denoted by C and activity coefficients by γ. Subscripts S and R indicate 'sea' and 'river'.

Activity coefficients are also dependent on the position in the cell and are obtained with the extended Debye–Hückel equation:

$$\gamma(x) = \exp\left[\frac{-0.51z^2\sqrt{I(x)}}{1 + (A/305)\sqrt{I(x)}}\right] \quad (12)$$

where γ is the activity coefficient of the ion, I the ion strength of the solution (mol/L), z the valency and A the effective hydrated ion radius in pm ($A_{Na^+} = 450$ pm and $A_{Cl^-} = 300$ pm).

The ionic strength I is calculated from the molar concentration C_i and the valency z_i of each ion. Because pure NaCl solutions are studied, the value of the ion strength is equal to the concentration in mol/L ($z_i^2 = 1$ for Na^+ and Cl^-). The factor 1000 is introduced to convert concentrations in mol/m^3 into the standard unit of mol/L as used usually in the ion strength.

$$I(x) = \frac{1}{2}\sum_i z_i^2\frac{C_i(x)}{1000} = \frac{C(x)}{1000} \quad (13)$$

The method holds for solutions to about 500 mol/m^3 (roughly the salt concentration in seawater).

From the molar conductivity Λ_m of a NaCl solution, the space-dependent area resistances of the sea and river water

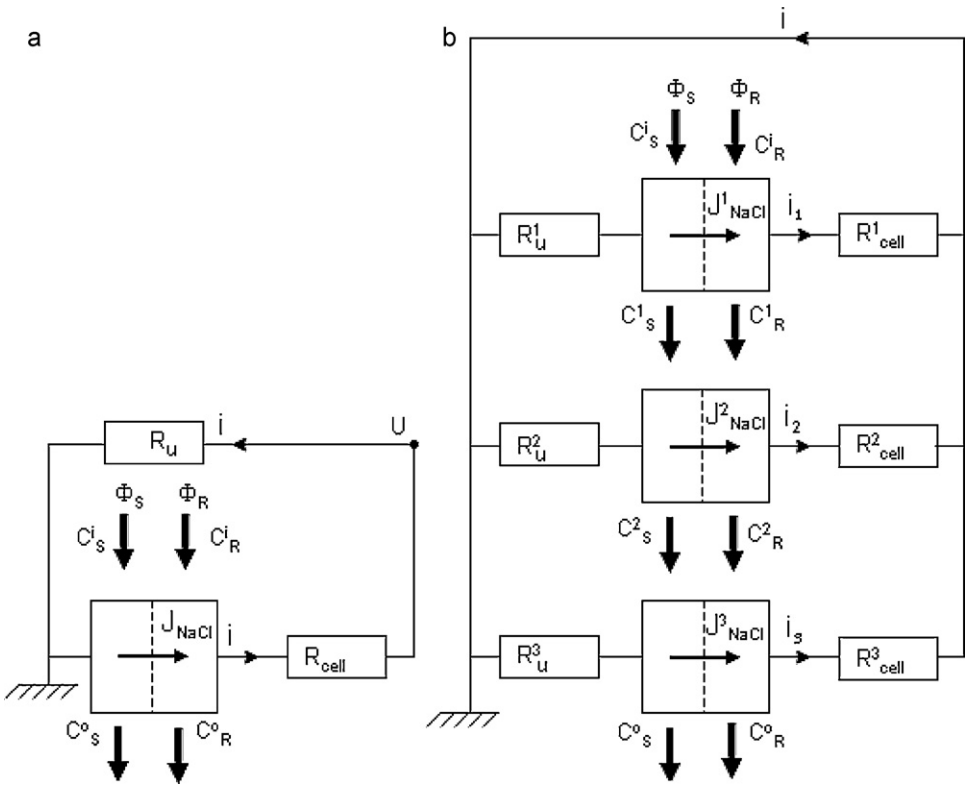

Fig. 3. A RED cell in co-current operation. (a) With undivided electrodes and one external load R_u and (b) With 3 separate electrodes and 3 external loads, $R^1{}_u$, $R^2{}_u$ and $R^3{}_u$. In the counter-current operation mode, the direction of the river water (Φ_R) is inverted.

compartments ($R_{a,S}(x)$ and $R_{a,R}(x)$) are calculated. In fact, Λ_m is dependent on the concentration C, but if a correct value of Λ_m is used for low concentrations, the calculated resistance of the river water compartment is reliable; the resistance of the seawater compartment, being much lower, has less influence on the total resistance:

$$R_{a,S}(x) = f\frac{\delta_S}{\Lambda_m C_S(x)} \tag{14}$$

$$R_{a,R}(x) = f\frac{\delta_R}{\Lambda_m C_R(x)} \tag{15}$$

In this equation, δ_S and δ_R are the thicknesses of the sea and river water compartment (Fig. 2). The obstruction factor f is a measure for the increase of the electrical resistance due to the negative effects of the spacer (tortuosity of the ion path, decrease of the amount conducting solution and shielding the membrane).

The area cell resistance is the sum of the compartment area resistances ($R_{a,S}(x)$ and $R_{a,R}(x)$) and the membrane area resistances (R_{AEM} and R_{CEM}) [20].

$$R_{a,cell}(x) = R_{a,S}(x) + R_{a,R}(x) + R_{AEM} + R_{CEM} \tag{16}$$

For maximal power, the external resistance (load) should be equal to the internal resistance [20]. Because the internal resistance of the cell is space-dependent, the load ($R_{a,u}(x)$) should also be space-dependent. This load – expressed in units of area resistance (Ωm^2) – is varying continuously in the x-direction:

$$R_{a,u}(x) = R_{a,cell}(x) \tag{17}$$

The current density (j) is now achieved with Ohm's law:

$$j(x) = \frac{E_{cell}(x)}{R_{a,cell}(x) + R_{a,u}(x)} \tag{18}$$

Salt transport from the sea to the river water compartment, J_{total}, is composed of a Coulombic part (J_{coul}) and a part due to co-ion transport, (J_{cit}). The Coulombic part is equal to j/F, where F is the Faraday constant (96,485 C/mol). The co-ion transport can be obtained from the NaCl diffusion constant for the membranes (D_{salt}), the membrane thickness (δ_m). The factor 2 is due to the fact that the there are two membranes in a cell.

$$J_{total}(x) = J_{coul}(x) + J_{cit}(x) = \frac{j(x)}{F} + \frac{2D_{\mathrm{NaCl}}}{\delta_m}[C_S(x) - C_R(x)] \tag{19}$$

This transport of NaCl causes changes in the sea and river water concentrations, determined by the mass balance equations:

$$\frac{d}{dx}C_S(x) = -\frac{b}{\Phi_S}J_{total}(x) \tag{20}$$

$$\frac{d}{dx}C_R(x) = \frac{b}{\Phi_R}J_{total}(x) \tag{21}$$

In these equations, Φ_S and Φ_R are the flow rates of sea and river water. In co-current operation, they have positive values; in the case of counter-current operation we assign a negative value to Φ_R.

The system – described by Eqs. (16)–(21) – is numerically solved with the program *Berkeley Madonna*. In the co-current mode, input concentrations $C_S(0)$ and $C_R(0)$ should be specified. In the counter-current mode (with a negative sign for the river water flow rate Φ_R) the significance of $C_R(0)$ in the model is the outlet concentration of the river water and the input concentration is given by $C_R(L)$; by adjusting $C_R(0)$ the specified input concentration $C_R(L)$ can be obtained.

Once the system is solved, the produced external power density function $P_d(x)$ is given by:

$$P_d(x) = \frac{1}{2}j^2(x)R_{a,u}(x) \tag{22}$$

The factor 1/2 is due to the double membrane area (CEM and AEM) in a cell. The total developed power P_{total} is obtained by inte-

gration over the length L in the x-direction:

$$P_{total} = b\int_0^L P_d\,dx \tag{23}$$

This results in an average power density ($\bar{P}_d$):

$$\overline{P_d} = \frac{P_{total}}{Lb} \tag{24}$$

Supply of feed water is expressed as flow rates Φ (m^3/s) or in velocities (m/s) or in the reverse unit residence time (t_R). For a compartment with dimensions L, b and δ:

$$v = \frac{\Phi}{Lb} \tag{25}$$

and

$$t_R = \frac{Lb\delta}{\phi} \tag{26}$$

2.4. Correction of the model for the effects of water flow through the membranes by osmosis

Opposite to the salt flux, there is a water flux (J_{water}) due to osmosis [16] of water from the river water compartment to the seawater compartment (analogous to the second term in Eq. (19)):

$$J_{water}(x) = -\frac{2D_{water}}{\delta_m}[C_S(x) - C_R(x)] \tag{27}$$

D_{water} stand for the diffusion constant of water in the membranes. The flux in Eq. (27) is expressed in mol m^{-2} s^{-1}. To convert this to a volumetric flux (J'_{water}), a factor M_{H_2O}/ρ_{H_2O} (molar mass over density) is added; in fact, this volumetric water flux is the superficial water velocity on the membrane.

$$J'_{water}(x) = -\frac{2D_{water}}{\delta_m}[C_S(x) - C_R(x)]\frac{M_{H_2O}}{\rho_{H_2O}} \tag{28}$$

The effect of salt transport on the concentrations in sea and river water is symmetric: If 0.1 g NaCl is transported from 1 L seawater (30 g/L) to 1 L river water (1 g/L), the new concentrations are 29.9 and 1.1 g/L: the decrease in seawater equals the increase in river water. On the other hand, if 100 mL water is transported by osmosis in the opposite direction, the new concentrations are 30/1.1 = 27.3 and 1/0.9 = 1.11 g/L. In this case the concentration change in the seawater is much larger than in the river water.

Osmosis affects – in principle – salt concentrations as well as feed water flow rates. The impact of the concentration change on the stack performance is much larger.

A typical value of the osmotic flux is about 10 mmol m^{-2} s^{-1} [16]. Assuming effective membrane length equal to 0.1 m, membrane-to-membrane distance 200 μm, and linear flow velocity 0.01 m/s the increment of linear flow velocity in the river water compartment is as low as 2%. This change is much smaller than the concentration change and therefore, we ignore the flow rate change during the passage of the cell and calculate only the effect on the concentration.

Fig. 4 shows the osmotic flow through a small area of membrane $dA = b\,dx$ of membrane to a thin slice in the seawater compartment. The osmotic flow rate is:

$$d\Phi_{osm} = bJ'_{water}\,dx \tag{29}$$

The incoming salt flow rate is $\Phi_S C_S$ (mol/s). This amount of salt also leaves the slice. Here, the concentration is given by:

$$C_S(x+dx) = \frac{\Phi_S C_S(x)}{\Phi_S + d\Phi_{osm}} = C_S(x)\frac{1}{1+(d\Phi_{osm}/\Phi_S)} \approx C_S(x)\left(1 - \frac{d\Phi_{osm}}{\Phi_S}\right) \tag{30}$$

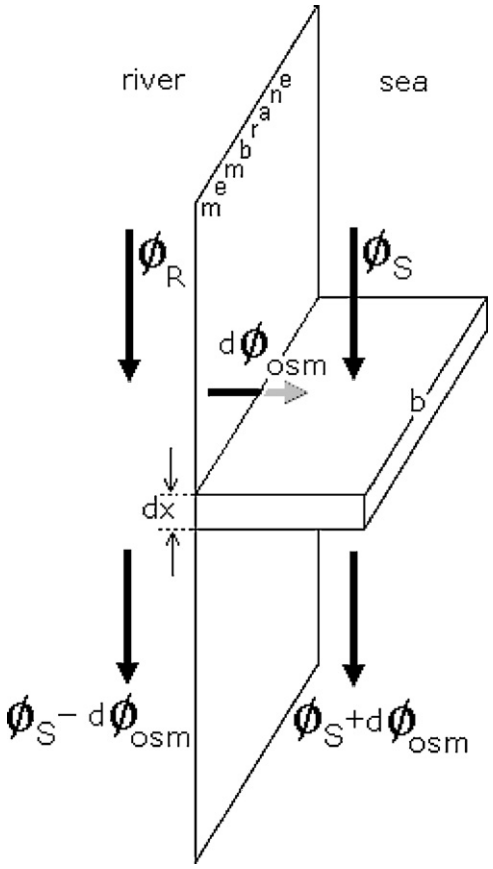

Fig. 4. Flow rate balance; an osmotic flow $d\Phi_{osm}$ is directed from the river water compartment (left) through the membrane to the seawater compartment (right).

$$dC_S(x) = -C_S(x)\frac{d\Phi_{osm}}{\Phi_S} = -C_S(x)\frac{bJ'_{water}}{\Phi_S}\,dx \tag{31}$$

For the increase of the salt content in the river water compartment, an analogous expression can be derived. To incorporate the effect of osmosis Eq. (28) should be added to the model (as described in Section 2.3) and Eqs. (20) and (21) should be replaced by:

$$\frac{d}{dx}C_S(x) = -\frac{b}{\Phi_S}J_{total}(x) - C_S(x)\frac{bJ'_{water}}{\Phi_S} \tag{32}$$

and by

$$\frac{d}{dx}C_R(x) = \frac{b}{\Phi_R}J_{total}(x) + C_R(x)\frac{bJ'_{water}}{\Phi_R} \tag{33}$$

2.5. Modeling of the system with undivided electrodes

The principle of this arrangement is shown in Fig. 3a. The left electrode (anode) is grounded and the potential on the cathode (right) is assigned to be U volt. In this way, the current through the cells is determined, and also the current through the external load and the delivered power in that load. In the model U is adjusted manually to maximal power in the load. The used program is a modification of the used program for an infinite number of electrodes. In the next section, the effect of segmentation on the performance of a RED stack will be shown.

3. Experimental

Two types of stacks were investigated: (1) the 'small stack' is described in detail elsewhere [15] with a functional membrane

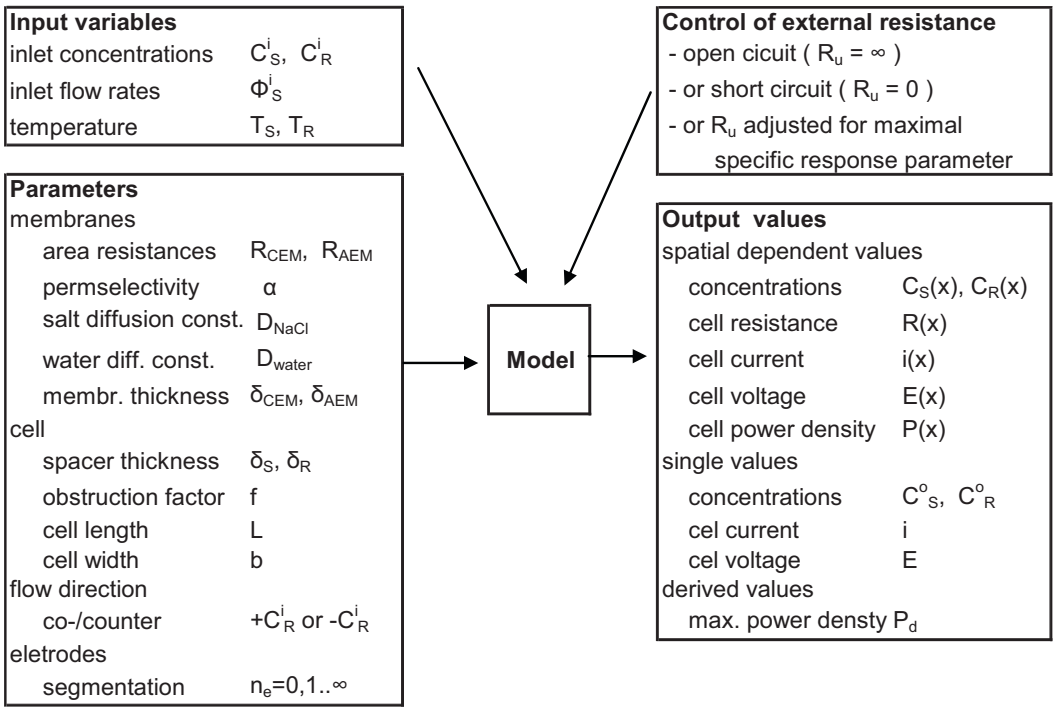

Fig. 5. Input variables and parameters as used by the model for calculating the outlet values.

area of 10 cm × 10 cm (50 cells) and (2) a novel 'large stack' of 25 cm × 75 cm (50 cells) with three electrode compartments – each with its own electrodes – were located on each side inside the endplates as described in [17]. Membranes used were Fumasep FKD cation exchange membranes, FAD anion exchange membranes (Fumatech, Germany) and Qianqiu Homogeneous AEM and CEM (Hangzhou Qianqiu Industry Co, China). The stacks were equipped with nylon woven spacers, thickness 200 μm (wire diameter 122 μm, porosity 67%) (Nitex 03–300/51, Sefar, The Netherlands); in some experiments with the small stack, 100 μm spacers (wire diameter 62 μm, porosity 74%) were used (Nitex 03–190/57). Gaskets were made of silicon microfilm with a thickness of 200 μm (SSF-MLTN-940, Specialty Silicone Fabricators, Paso Robles, USA).

In our experiments, 'seawater' consisted of 30 g NaCl/L and 'river water' of 1 g NaCl/L. The salinity of our artificial 'seawater' is comparable to real seawater: for oceans, this is about 35 g/L and for water in the North Sea near to the Dutch coast it is 32 g/L. The mean salinity of the river Rhine is 0.135 g/L; we chose a rather high value of 1 g/L to obtain stable experimental results.

4. Model validation with laboratory scale experimental set-ups

Fig. 5 shows the input variables and process parameters of the model. In general, most parameters are well defined but some are less reliable: the obstruction factor of the spacers (f) and the diffusion constants for salt (D_{salt}) and water (D_{water}). These parameters are found by fitting the model to experimental data. The obstruction factor (also known as 'shadow factor') describes the extra electrical resistance of the water compartments due to the influence of the spacer [14–16,24,25]. The spacer effect includes: (i) the increase of the electrical resistance due to the tortuosity of the ion path, (ii) decrease of the amount conducting salt solution in the compartments and (iii) the shielding effect of the spacer on the membrane on the contact places. D_{salt} and D_{water} should only describe the diffusion of ions and water in the membrane; however in practice also leakage (around the inlet holes) can contribute to these diffusion constants.

For the calibration, we used three small stacks (10 cm × 10 cm) with Qianqiu homogeneous membranes (25 cell, with cross-current feed). For the fitting procedure the residue was calculated from the maximal power density (P_d) and the outlet concentrations under open circuit conditions (no external load connected to the system) of the seawater (C_S^{open}) and river water (C_R^{open}):

$$\text{Residue} = \sum_i (\Delta P_{d,i})^2 \sum_i \left(\Delta C^{\text{open}}_{S,i}\right)^2 \sum_i \left(\Delta C^{open}_{R,i}\right)^2 \quad (34)$$

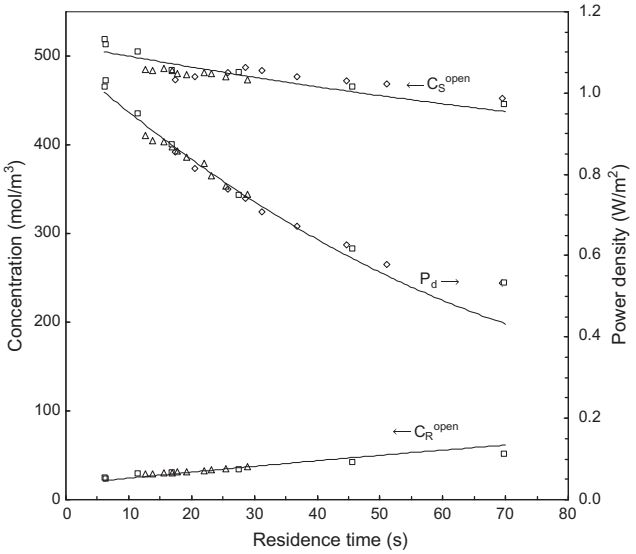

Fig. 6. Calibration of the model. Computed (line) and measured (marked points) power densities and outlet concentrations of three small Qianqiu stacks of 25 cells as function of the residence time. Power densities (P_d) are measured under maximal power conditions; outlet concentrations (C_R^{open} and C_S^{open}) were determined with open circuit (unloaded) stacks. Different marks (□, △ and ◇) refer to different stacks.

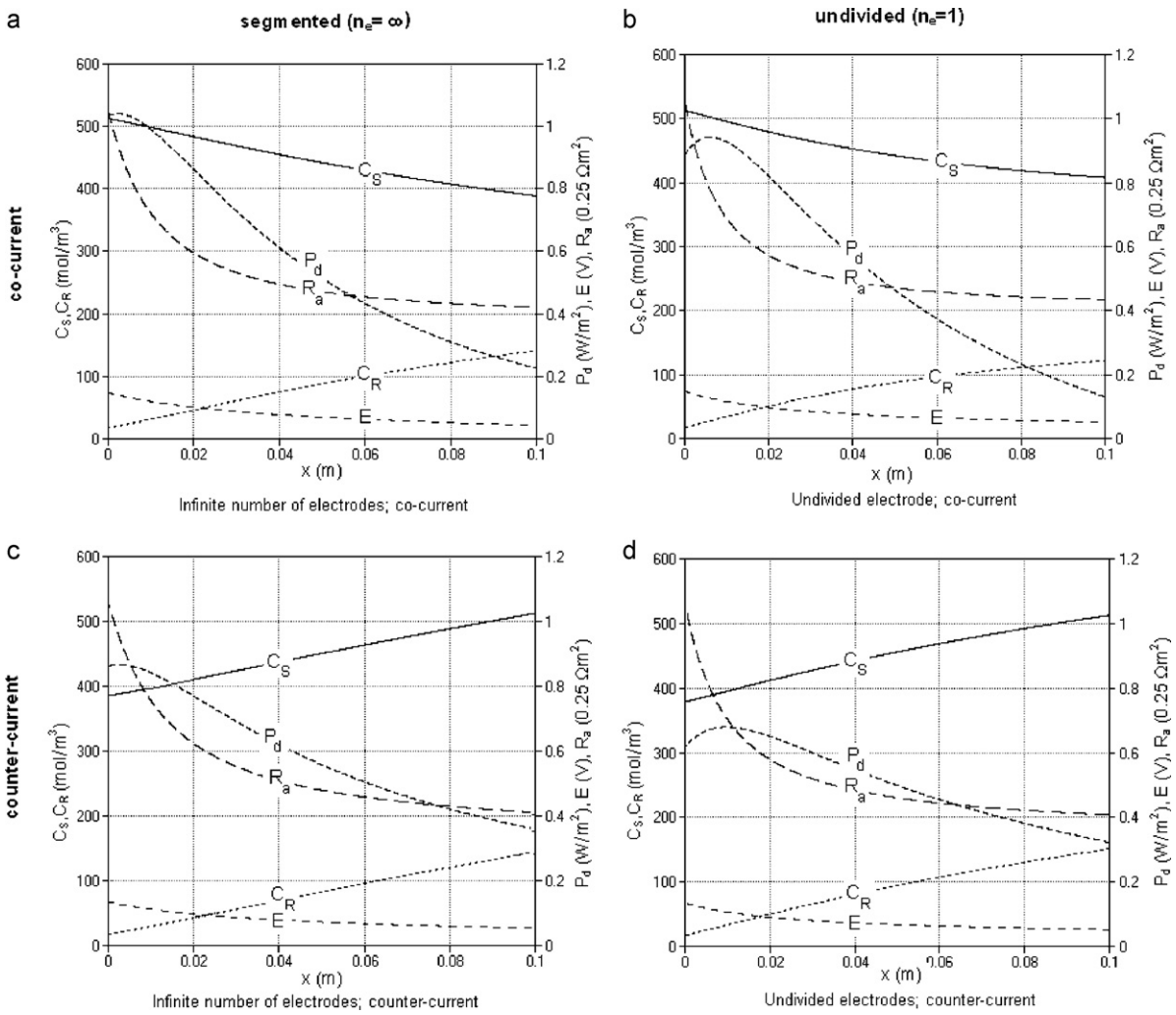

Fig. 7. Model predictions for a stack with Fumasep membranes. Dimensions of the stack: 10 cm × 10 cm; spacer thickness 200 μm. A residence time of 60 s is used in the calculation. In each graph the following local values are shown: the concentration of seawater (C_S) and river water (C_R), (left axis), power density (P_d), open circuit voltage (E) and area resistance (R_a), (right axis). The graphs show the effects of the relative flow direction and of the segmentation of the electrodes. The two left graphs (a and c) are related to systems with a high degree of segmentation of the electrodes; the right two graphs (b and d) to systems with undivided electrodes. The upper two graphs (a and b) describe the behavior of co-current feed and the lowest two (c and d) of counter-current feed.

In this equation, $\Delta P_{d,i}$ is the difference of the measured and calculated power density, etc. We calibrated the model by adjusting the parameters f, D_{salt} and D_{water} until the minimal residue was achieved.

Fig. 6 shows (i) the measured and fitted values of the maximal power density of the stack under condition of maximal power, (ii) the measured and fitted outlet concentrations of the unloaded stack. The fitted values are near to the experimental data used as start values. The following values are found: obstruction factor f = 1.6 (starting value 1.7 from [15]), salt diffusion constant $D_{salt} = 2.5 \times 10^{-11}$ m^2/s (start value 3.2×10^{-11} m^2/s from [16]) and water diffusion constant $D_{water} = 3.5 \times 10^{-9}$ m^2/s (starting value 7.9×10^{-9} m^2/s from [16]). Both start values and fitted values are in the normal range of diffusion constants in ion exchange membranes [16].

In fact the model is developed for co- or counter-current operation and in contrast, in the small stack the relative directions of the sea and river water flows are perpendicular (cross-current operation). In Section 5.2 it will be shown that differences between co- and counter-current operation are small. Therefore, it is reasonable to use the model also for the small stack because cross-current operation can be regarded as an intermediate between the co- and counter-current operation.

5. Application of the electrical model for optimization of the water compartments

5.1. Spatial effect within the cell

To give a first impression of the behavior within a RED cell, the (not yet calibrated) model is used to simulate a small cell (10 cm × 10 cm), equipped with Fumasep membranes (FAD and FKD). Used parameters as obtained from precious work [15] include: obstruction factor: f = 2, membrane area resistances: $R_{CEM} = 5.90 \times 10^{-4}$ Ωm^2 and $R_{AEM} = 1.63 \times 10^{-4}$ Ωm^2, permselectivity: α = 0.88, spacer thickness (both compartments): $\delta_S = \delta_R$ = 200 μm and NaCl diffusion coefficient: $D_{salt} = 0.13 \times 10^{-10}$ m^2/s. Input salt contents are 30 g/L (512.8 mol/m^3) for the seawater and 1 g/L (17.1 mol/m^3) for the river water; residence time is 60 s for sea and for river water.

Fig. 7 shows some local variables of cells with: (a) segmented with an infinite number of electrodes and co-current operation, (b) undivided electrodes and co-current operation, (c) segmented with an infinite number of electrodes and counter-current operation, and (d) undivided electrodes and counter-current operation. Plotted are local concentrations in the sea ($C_S(x)$) and in the river water compartments ($C_R(x)$), together with local power density ($P_d(x)$),

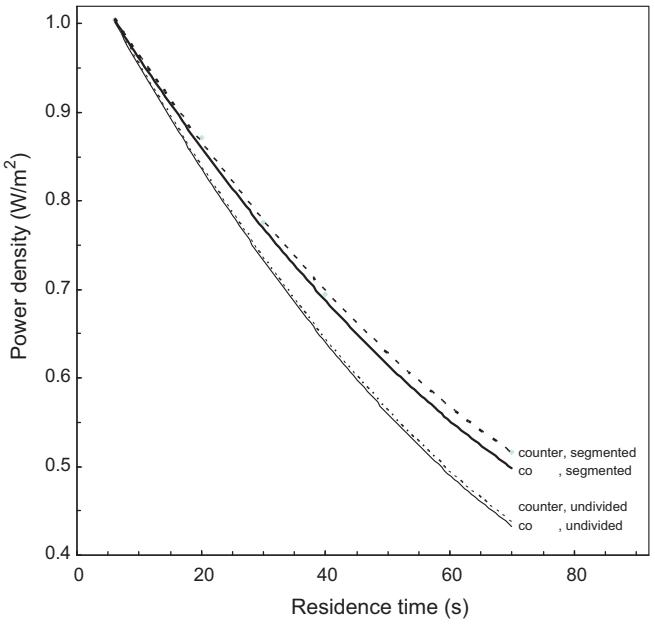

Fig. 8. Computed power densities for different flow directions (co-current and counter-current) and different electrodes (undivided and infinite segmented).

local open circuit voltage ($E(x)$) and local area resistance ($R_a(x)$). In each graph, the river water inlet is on the left side. In the co-current mode graphs (a and b) the seawater inlet is also on the left side. In the counter-current graphs (c and d), the seawater inlets are on the right side. Effects of osmosis are not incorporated in this model and therefore the graphs of the concentration in sea and river water (C_R and C_R) are symmetrical.

The graphs show the following aspects of the cell behavior; going from the river water inlet to the river water outlet (from left to right) we note:

- The salt concentrations in the sea and river water compartments (C_S and C_R) change more or less linearly.
- The electrical resistance (R_a) decreases sharply in the first quarter of the flow path and after that more slowly.
- The cell voltage decreases smoothly to about half the initial value.
- The generated power density (P_d) is maximal short after the river water inlet. The reason is that the input concentration of the river water is very low and the resulting high resistance limits the electrical current and thereby the power. In the models with undivided electrodes (plots b and d) this maximum is a bit delayed.
- With the segmented electrodes (plots a and c) the power density is higher over the whole length of the cell than with the undivided electrodes (plots b and d).

5.2. Evaluation of the flow direction (co-current and counter-current)

Fig. 8 shows computed data for two different flow directions (co- and counter-current) and two different electrode systems (undivided and segmented). Used are the values for the Qianqiu homogeneous membranes with spacers (sea and river) of 200 μm. The effect of the flow direction is small. For undivided electrodes, the differences are less than 1% in the studied residence time range. For the system with infinite segmented electrodes, the benefit of counter-current flow is maximally 2% better at longer residence times (70 s).

Measured data [17] show a slightly higher power density for co-current operation (4%) whereas the model shows no significant differences. This could be explained by the fact that the model is based on a rigid stack but the real stack is flexible. Counter-current operation introduces high local pressure differences between sea- and river water compartments. This can result in local obstructions for the fluid flow and in local deviations of the electrical conductivity [17].

By taking into consideration that co-current operation causes smaller local pressure differences between the river and seawater compartments – hence smaller risk of leakages and the possibility to use very thin membranes with high fluxes and very open spacer structures with low hydrodynamic resistance – it was decided to focus on co-current design.

Table 1
Average maximal power density (P_d) as function of the number of segments of the electrode. Added is the gain achieved by dividing process. Each segment has its own load, optimized for maximal power output.

Segments	P_d (W/m^2)	Gain (%)
1	0.434	0.0
2	0.490	12.9
3	0.502	15.7
4	0.505	16.4
5	0.506	16.6

5.3. Benefit of the system with segmented electrodes

Experimentally, an increase of 11% is found (from 0.441 to 0.488 W/m^2) by dividing the electrode into three independent segments, each loaded with its own optimal resistance [17]. As shown in Fig. 8, the model forecasts also an increase of the power density by segmentation of the electrodes. The benefit of a system with an infinite segmentation and operated in the co-current mode, is according to Fig. 8 about 15% at a residence time of 70 s. The increase in power is attributed to the equal external resistance which matches the internal stack resistance (Eq. (17)) of the segment. By adding more segments with adjusted external resistances more power can be generated.

However, the model uses infinite segmented electrodes whereas the experiments were performed with electrodes divided into only three segments. Therefore, we briefly discuss the effect of the degree of segmentation to the power density. The results are shown in Table 1. Dividing the electrodes into some segments can be useful. A disadvantage of the use of segmented electrodes is the necessity to use an optimized load for each segment.

5.4. Design optimization of thicknesses and lengths of the water compartments and of the resident times

Key parameters in the design of a RED stack are the thicknesses and the length of the sea and river water compartments. In most experiments with our small stack we used a spacer thickness of 200 μm for both compartments. In this case the electrical cell resistance is mainly determined by the river water compartment; the hydrodynamical loss with the used spacers is about 20% [15]. With thinner spacers the electrical resistance (perpendicular on the spacers) decreases but at the cost of a higher hydrodynamical resistance in the lateral direction.

It is not self-evident that optimal performance is achieved with equal spacers for both compartments. It seems reasonable that the spacer thickness of the seawater compartment can be taken some (e.g. 5) times thicker than that of the river water compartment. In this case the total electrical cell resistance is hardly influenced; on the other hand the hydrodynamic resistance of the seawater compartment is much lower than that of the river water compartment. In this way the total hydrodynamical loss is reduced to about half. A thicker seawater compartment permits also the use of a seawater

Table 2
Cell D: cell with real membranes and real spacers.

Qianqiu membrane; real spacer $f = 1$													
L (m)	δ_S (μm)	δ_R (μm)	$t_{R,S}$ (s)	$t_{R,R}$ (s)	v_S (cm/s)	v_R (cm/s)	C'_S (mol/m^3)	C'_R (mol/m^3)	Φ_S/Φ_R	P_d (W/m^2)	P_{d-hydr} (W/m^2)	P_{d-net} (W/m^2)	Z_{net} (kJ/m^3)	$R_P{}^Z$
α. Maximization of P_{d-net}														
0.010	*194*	*96*	*5.2*	*2.3*	0.19	0.43	492	33	0.90	1.78	0.14	**1.63**	78	128
0.025	*280*	*137*	*10.1*	*4.8*	0.25	0.52	487	38	0.98	1.52	0.14	**1.38**	97	134
0.050	*373*	*181*	*17.0*	*8.5*	0.29	0.59	483	43	1.03	1.32	0.14	**1.18**	111	131
0.100	*503*	*240*	*28.6*	*15.2*	0.35	0.66	478	49	1.11	1.13	0.13	**0.99**	126	125
0.250	*753*	*356*	*58.2*	*33.3*	0.43	0.75	471	58	1.21	0.88	0.12	**0.76**	142	109
0.500	*1030*	*486*	*100.3*	*60.7*	0.50	0.82	466	65	1.28	0.71	0.11	**0.61**	151	91
1.000	*1430*	*672*	*175*	*112*	0.57	0.89	459	74	1.36	0.56	0.09	**0.47**	156	73
β. Maximization of $R_P{}^Z$														
0.010	*240*	*54*	*5.9*	*7.7*	0.17	0.13	497	92	5.76	1.08	0.03	1.05	298	**313**
0.025	*341*	*88*	*11.4*	*14.1*	0.22	0.18	493	96	4.79	0.97	0.03	0.94	300	**281**
0.050	*448*	*124*	*18.8*	*22.1*	0.27	0.23	489	101	4.25	0.88	0.04	0.84	300	**252**
0.100	*590*	*175*	*31.3*	*35.5*	0.32	0.28	485	106	3.82	0.78	0.04	0.74	299	**220**
0.250	*863*	*274*	*62.6*	*68.0*	0.40	0.37	478	114	3.42	0.64	0.04	0.59	294	**174**
0.500	*1160*	*388*	*107*	*114*	0.47	0.44	472	122	3.19	0.53	0.04	0.48	285	**138**
1.000	*1590*	*553*	*186*	*196*	0.54	0.51	466	130	3.03	0.43	0.04	0.38	272	**104**

Effect of the length of the flow path (L) on different cell parameters. Cell specifications: undivided electrodes, co-current flow direction, spacerless compartments, ideal membranes. Inlet concentrations: 512.8 and 17.1 mol/m^3. Maximized values (in bold) are the power density (P_{d-net}) in the upper part (α) and the response product $R_P{}^Z$ in the lower part (β). Adjusted values (italics) include: compartment thicknesses (δ_S and δ_R) and residence times ($t_{R,S}$ and $t_{R,R}$). Normal printed values are calculated and include: linear average velocities (v_S and v_R), outlet concentrations (C'_S and C'_R), flow rate ratio (Φ_S/Φ_R), electrical power density (P_d), hydrodynamic loss (P_{d-hydr}), net power density (P_{d-net}), net river water yield (Z_{net}), response product ($R_P{}^Z$) and the Reynolds numbers (Re_S and Re_R).

flow rate that is higher than the river water flow rate: the amount of harvested energy per m^3 river water can increase from 1.8 MJ with a 1:1 ratio to 2.6 MJ with a large surplus of seawater [15]. However, a thicker seawater compartment may increase losses due to the increased parasitic ionic currents [20].

A special property of the hydrodynamic loss is that it is affected by the length of the flow path L. If some ions diffuse (and generate energy) only in the second part of the flow path, these ions (together with the accessory amount of water) have traveled the first part in vain, only causing frictional losses there. Therefore L is a main design parameter.

The main finding in Sections 5.2 and 5.3 was that a stack in co-current operation with undivided electrodes is a good choice. Based on this configuration, we used the developed RED model for cells with two types of membranes and two spacer configurations. For each investigated cell we study the influence of the flow path length on the various response parameters, power density and energy efficiency. For each length, thicknesses of both compartments and flow rates of both feeds are adjusted for maximal output of the different response parameters.

To study the influence of the flow path length, to find the theoretical limits of the performance and to quantify the contribution of the membranes and spacers to the losses, we continue the calculations, using with the response parameters P_{d-net} (net power density) and $R_P{}^Z$ (response product; $R_P{}^Z = Z_{net}P_{d-net}$) for the optimization. We did not use Z_{net} (net river water yield) for maximization because this resulted in extremely long residence times and very low power densities. A compromise between net power density and net efficiency is the response product ($R_P{}^Z$). We shall refer to the maximization of the net power density (P_{d-net}) as α-mode and to maximization of the response product ($R_P{}^Z$) as β-mode.

We used the model to determine the performance of four cell configurations:

(A) without spacers and with ideal membranes
(B) with real spacers and with ideal membranes
(C) without spacers and with real membranes
(D) with real spacers and with real membranes

The ideal membranes have no electrical resistance, no osmosis and no co-ion transport (i.e. a permselectivity $\alpha = 1$). The real membranes are the Qianqiu homogeneous membranes. For spacerless cells, there is supposed to exist a laminar flow between the membranes. The real spacers are similar spacers to those studied in [17].

In order to compare the four cell configurations in a similar way, in each configuration was used an obstruction factor $f = 1$, a flow path length $L = 0.25$ m and input concentrations $C_S = 512.8$ and $C_R = 17.1$ mol/m^3 (i.e. 1 and 30 g/L).

5.4.1. Cell configuration A: design optimization of flow channel dimensions without spacers and with ideal membranes

Normally, spacers are used between the membranes. They are used for mechanical stability of the stack and may furthermore promote mixing within the compartments, thereby reducing the thickness of the diffusion layers. However, in our ideal hydrodynamic model we ignore the effect of spacers in the compartments. Reynolds numbers can be determined as follows:

$$Re = \frac{vD\rho}{\mu} \tag{35}$$

where v is the mean velocity, D the hydraulic diameter, ρ the density of the feed water and μ the dynamic viscosity (0.9×10^{-3} Pa s for pure water at 25 °C). For a flow between two parallel planes, the hydraulic diameter equals two times the distance between

Table 3
Main properties of the cell configurations A–D. Data are tabulated for two cell lengths (L = 0.01 m and for 1 m) and for two maximization modes (maximization of P_{d-net} and $R_P{}^Z$).

Cell configuration spacer membranes		A, none, ideal		B, real, ideal		C, none, Qianqiu		D, real, Qianqiu	
Cell length (m)		0.001	1	0.001	1	0.001	1	0.001	1
α. Maximization of P_{d-net}									
Net power density	P_{d-net} (W/m^2)	60.2	6	11.6	1.2	2.4	1.3	1.6	0.5
Net river water yield	Z_{net} (kJ/m^3)	371	373	373	373	32	105	78	156
Flow ratio	Φ_S/Φ_R	2.8	2.8	1.5	1.5	0.8	1	0.9	1.4
Thickness seawater comp.	δ_S (μm)	19	185	96	965	56	331	194	1430
Thickness river water comp.	δ_R (μm)	9	92	48	478	29	160	96	672
β. Maximization of $R_P{}^Z$									
Net power density	P_{d-net} (W/m^2)	51.6	5.2	10	1	1.3	0.9	1.1	0.4
Net river water yield	Z_{net} (kJ/m^3)	557	555	555	554	290	300	298	272
Flow ratio	Φ_S/Φ_R	2.4	2.4	2.9	2.9	13.9	4.5	5.8	3.3
Thickness seawater comp.	δ_S (μm)	23	232	121	1200	75	398	240	1590
Thickness river water comp.	δ_R (μm)	9	89	46	461	11	108	54	553

them. Applying Eq. (35) to a standard small cell as described in [15] (dimensions 0.1 cm × 0.1 m with a compartment thickness of 200 μm), we obtain for a relative short residence time of 5 s (corresponding to a mean velocity of 2 cm/s) a Reynolds number of 4.4, low enough to be sure of a laminar flow.

With a laminar flow between the membranes, the pressure drop over the sea and river water compartment (ΔP_S and ΔP_R) is:

$$\Delta P_S = \frac{2\mu L \Phi_S}{b\delta_S^3}, \quad \Delta P_R = \frac{2\mu L \Phi_R}{b\delta_R^3} \tag{36}$$

The hydraulic power loss P_{hydr} is then

$$P_{hydr} = \Delta P_S \Phi_S + \Delta P_R \Phi_R \tag{37}$$

The second assumed ideality of the cell is that they are equipped with membranes without electrical resistance and with permselectivity $\alpha = 1$ and no osmosis.

5.4.2. Cell configuration B: design optimization of flow channel dimensions with real spacers and ideal membranes

We will compare the pressure drop in spacer filled systems with spacerless systems. Therefore we extend Eq. (37) (describing the pressure drop in a spacerless compartment) with a factor Q. In this way Eq. (38) is obtained, which describes the pressure drop in a spacer filled system:

$$\Delta P = Q \frac{2\mu L \Phi}{b\delta^3} \tag{38}$$

From formerly experiments [17] the hydraulic properties of a special woven polyamide spacer is determined experimentally with a large stack containing 50 cells (compartment thickness δ = 200 μm, stack width b = 0.75 m and length of the flow path L = 0.25 m). The pressure drop in this stack was correlated with the flow rate: $\Delta P = 1.0 \times 10^9\, \Phi$. From Eq. (39) a value of Q = 715 is derived.

The used spacer in [17] was of the 'balanced plain weave' type: warp and weft are made of threads of the same size at the same distance and are indistinguishable in the fabric. We will restrict ourselves to similar spacers of this type. It is reasonable to assume that the resistance through the spacer in the lateral direction is – as in the case of the spacerless compartment – proportional to the third power of the thickness. Therefore, we can use Eq. (38) for the pressure drop over compartments with similar spacers with thickness δ. For pure water at 25 °C, Eq. (38) becomes:

$$\Delta P = 1.3 \frac{L\Phi}{b\delta^3} \tag{39}$$

With this pressure drop the calculations of cell configuration A are repeated. In this model we use again "ideal membranes" and ignore also any shielding, consequently f = 1.

5.4.3. Cell configuration C: design optimization of flow channel dimensions without spacers and with real membranes

To investigate the effect of the membranes, a model is used with Qianqiu homogeneous membranes without spacers. Membrane values are used as described in [16].

5.4.4. Cell configuration D: design optimization of flow channel dimensions with real spacers and real membranes

Now the complete real cell configuration is used: a cell with Qianqiu homogeneous membranes and with real spacers. In fact, the cell configurations A and B are combined in this cell configuration. In Table 2 the results are listed. It can be concluded that:

- Short cells perform better than long cells on power density.
- Net power density and net river water yield are counteracting in the α-mode; in the β-mode the net river water yield is almost independent of the cell length.
- In all cases (for different values of the cell length L; for the α-mode as well as for the β-mode) the optimized seawater spacers are 2–4 times thicker than the river water spacers.
- For maximal power density, the flow rate ratio (Φ_S/Φ_R) is about unity; for maximal river water the optimal value of this ratio is much more.

We repeated the optimization procedure with cell configuration D by maximization of $R_P{}^Z$ with fixed spacer thicknesses as found at the maximization of P_{d-net}. Under these conditions we achieved a net power density and a net river water yield quite near the values achieved with optimized spacer thicknesses. This is an important finding. The conclusion is that a RED cell as designed for maximal net power output also can be used for maximal $R_P{}^Z$, only by adjusting the flow rates of the sea and river water.

In the next paragraph we will discuss the four models and give general conclusions.

5.5. Comparison of the four models for optimal cell parameters

It is useful to compare the results of the four discussed cell configurations. In Table 3 the main results are listed for these four cell configurations (A–D) and the two optimizing modes (α-mode: optimized for maximal net power density, P_{d-net} and β-mode: optimized for maximal response product, $R_P{}^Z$). The results include net power density, net river water efficiency, flow rate ratio and the thicknesses of the compartments. Tabulated are the two values as achieved at the two extreme values of the flow path length as used in our calculations (L = 0.01 m and 1 m).

From Table 3 it can be concluded:

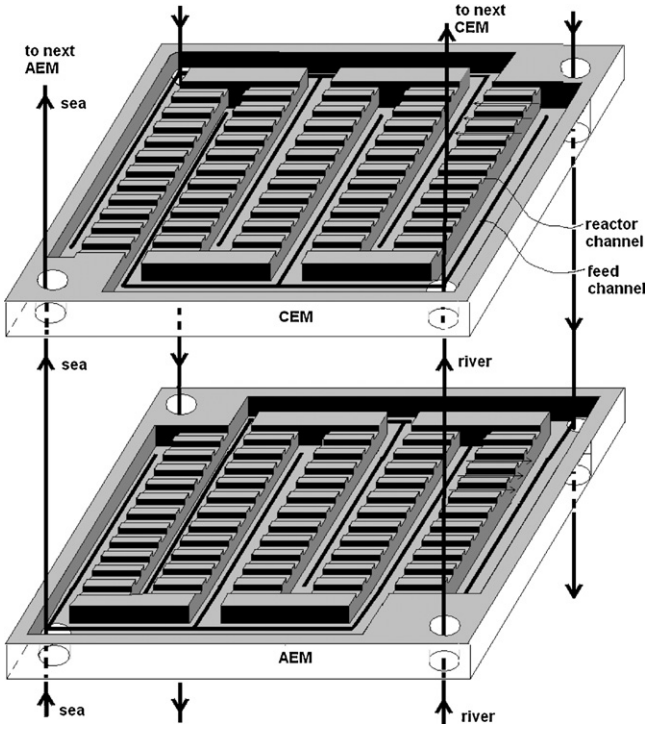

Fig. 9. A RED cell with fractal profiled membranes. Feed channels are pressed in the membranes (thickness 0.5 mm) until a depth of 0.4 mm. Compartments are pressed with a depth of 0.1 mm. All cell dimensions are arbitrary, for illustration only.

(a) *Membranes and spacers.* Membranes should have a minimal electrical resistance and spacers a minimal hydrodynamic resistance. The cell equipped with ideal membranes and real spacers (cell configuration B) performs better with respect to net power density and net river water yield than a cell equipped with Qianqiu membranes without spacers (cell configuration C). It can be concluded that improvements of the membranes have more effect on power density and efficiency than improvements of the spacer.
(b) *Flow path length L.* The crucial parameter is the flow path length L, it should be very short. It is difficult to incorporate very short values of L within the concept of classical plate-and-frame stacks: a stack with hundreds of cells (e.g. resulting in a height of 1 m) and very short flow path (e.g. 5 cm or shorter) is mechanical very instable. The same holds for spiral wound modules as designed for normal electrodialysis. Another approach – using fractal spacers – is discussed in Section 5.6.
(c) *Mode (α or β).* In the α-mode, very short values of the flow path (L) result in low river water yields (Z_{net}). However, in the β-mode the influence of L on Z_{net} is minimal. Moreover, values of Z_{net} are substantial larger than in the α-mode.

5.6. Novel compartment and cell design

Post et al. [26] showed that it is possible to generate energy from sea and river water with RED at a price comparable with the price of wind energy. They based their calculations on the assumption of a power density of 2 W/m^2 and an energy recovery of 70% (equivalent to a river water yield of 1.1 MJ/m^3). Our values with real membranes and real spacers (cell configuration D, Table 2) are much lower (1.6 W/m^2 and 0.08 MJ/m^3 in the α-mode or 1.1 W/m^2 and 0.30 MJ/m^3 in the β-mode) and it is obvious that the current spacers and membranes should be improved for use in economical operated RED stacks. One solution is to integrate membranes and spacers. Brauns suggested to use corrugated membranes in a RED stack to avoid the use of spacers [27].

With the following reasoning, we arrived at the concept of fractal design. The reasoning points are:

(a) Compartments in current systems have two functions: they act as feed channels and as reactors. The first function requires thick and the other thin compartments. Therefore, both functions should be decoupled by a spatial separation between the supply part and the reactor part.
(b) The electrical specific resistance of seawater is comparable with ion exchange membranes and the specific resistance of river water is much higher. Therefore the most profits are achievable by decreasing the thickness of the river water compartment.
(c) Spacers are unwanted due to their large hydrodynamic resistance.
(d) The shorter the channel length, the higher the produced power density.

These arguments lead to the concept of fractal profiled membranes. Fig. 9 shows a complete RED cell with a profiled AEM (beneath; serving as seawater compartment) and a profiled CEM (above; serving as river water compartment). To form an idea, the following dimensions can be imagined: the membrane thickness is 0.5 mm, in the membranes are pressed the feed channels with a depth of 0.4 mm and the reactor cannels with a depth of 0.1 mm. In the river water compartment, the electrical resistance is decreased by the use of thin compartments (0.1 mm). The reactor channels are short, and spacerless, and have a low hydrodynamic resistance. Because of the low electrical resistance of the seawater, the reactor channels in the seawater compartment can be deeper. A patent with all details is submitted.

6. Conclusions

A process model is developed and validated for laboratory experimental RED systems. The model is used to study response parameters, suitable for optimization purposes. It was found that there are two response parameters that give useful results on maximization: first the net power density and second the product of power density and net river water yield. A RED stack as designed for maximal net power density is also suitable for a high river water yield. In this case other flow rates should be applied with an excess of seawater. It is reasonable to suppose that when the first economical RED plants are built, there is enough fresh water and high power density is more wanted than high river water yield. Therefore, a RED plant can be operated on high power density initially and a more energy efficient mode can be used eventually.

Theoretical, performance of co-current and counter-current operation is almost identical. However, experimentally a 4% power increase for co-current operation was observed. Therefore, co-current operation is preferred. Moreover, in this mode the local pressure differences between the compartment are very low, which enables the use of very thin membranes and very open spacers. Thin membranes have a low electrical resistance but lack mechanical strength; open spacers have a low hydrodynamic resistance but are compressible. An extra benefit of the low pressure differences is that leakage through pinholes in the membranes and around the inlet and outlet holes is minimal.

Segmentation of the electrodes can increase the power density with about 15%. If divided into two parts, most of this percentage is achieved. The same effect can be achieved – in principle – with two separate RED modules; for an optimal result, the length of the flow channel of both stages should be half the length of the original stack.

The model showed the huge negative influence of channel length on power density, the need for thin membranes with a low electrical resistance and the requirement of spacers with a very open structure (or no spacers at all). Therefore, fractal profiled membranes are very promising. They do not require spacers, the membrane is locally very thin, and the fractal structure allows larger cell dimensions.

Acknowledgements

This work was performed in the TTIW-cooperation framework of Wetsus, centre of excellence for sustainable water technology (www.wetsus.nl). Wetsus is funded by the Dutch Ministry of Economic Affairs, the European Union Regional Development Fund, the province of Fryslân, the city of Leeuwarden and the EZ/Kompas program of the "Samenwerkingsverband Noord-Nederland". The first author thanks the NHL Hogeschool who facilitated this research by detaching him to Wetsus and the participants of the theme "Energy" theme for their fruitful discussions and their financial support.

References

[1] R.E. Pattle, Production of electric power by mixing fresh and salt water in the hydroelectric pile, Nature 174 (1954) 660.
[2] R.E. Pattle, Electricity from fresh and salt water—without fuel, Chem. Proc. Eng. 35 (1955) 351–354.
[3] J.T. Kuleszo, The Global and Regional Potential of Salinity-Gradient Power, Dept. Environmental Sciences, Environmental Systems Analysis Group, Wageningen University and Research centre, 2008.
[4] G.L. Wick, W.R. Schmitt, Prospects for renewable energy from sea, Mar. Technol. Soc. J. 11 (1977) 16–21.
[5] Energy Information Administration, http://www.eia.doe.gov.
[6] J.W. Post, J. Veerman, H.V.M. Hamelers, G.J.W. Euverink, S.J. Metz, K. Nymeijer, C.J.N. Buisman, Salinity-gradient power: evaluation of pressure-retarded osmosis and reverse electrodialysis, J. Membr. Sci. 288 (2007) 218–230.
[7] R.E. Lacey, Energy by reverse electrodialysis, Ocean Eng. 7 (1980) 1–47.
[8] J.N. Weinstein, F.B. Leitz, Electric power from differences in salinity: the dialytic battery, Science 191 (1976) 557–559.
[9] J. Jagur-Grodzinski, R. Kramer, Novel process for direct conversion of free energy of mixing into electric power, Ind. Eng. Chem. Process Des. Dev. 25 (1986) 443–449.
[10] R. Audinos, Electrodialyse inverse, Etude de l'energie electrique obtenue a partir de deux solutions de salinites differentes, J. Power Sources 10 (1983) 203–217.
[11] R. Audinos, Electric power produced from two solutions of unequal salinity by reverse electrodialysis, Ind. J. Chem. 31A. (1992) 348–354.
[12] M. Turek, B. Bandura, Renewable energy by reverse electrodialysis, Desalination 205 (2007) 67–74.
[13] F. Suda, T. Matsuo, D. Ushioda, Transient changes in the power output from the concentration difference cell (dialytic battery) between seawater and river water, Energy 32 (2007) 165–173.
[14] J.W. Post, H.V.M. Hamelers, C.J.N. Buisman, Energy recovery from controlled mixing salt and fresh water with a reverse electrodialysis system, Environ. Sci. Technol. 42 (2008) 5785–5790.
[15] J. Veerman, S.J. Metz, M. Saakes, G.J. Harmsen, Reverse electrodialysis: performance of a stack with 50 cells on the mixing of sea and river water, J. Membr. Sci. 327 (2009) 136–144.
[16] J. Veerman, R.M. de Jong, M. Saakes, S.J. Metz, G.J. Harmsen, Reverse electrodialysis: comparison of six commercial membrane pairs on the thermodynamic exergy efficiency and power density, J. Membr. Sci. 343 (2009) 7–15.
[17] J. Veerman, M. Saakes, S.J. Metz, G.J. Harmsen, Electrical power from sea and river water by reverse electrodialysis: a first step from the laboratory to a real power plant. Environ. Sci. Technol. in press, doi:10.1021/es1009245.
[18] C. Forgacs, Generation of electricity by reverse electrodialysis, BGUN-RDA – 178-78 Ben-Gurion University, Israel, 1978.
[19] C. Forgacs, R.N. O'Brien, Utilization of membrane processes in the development of non-conventional renewable energy sources, Chem. Can. 31 (1979) 19–21.
[20] J. Veerman, J.W. Post, S.J. Metz, M. Saakes, G.J. Harmsen, Reducing power losses caused by ionic shortcut currents in reverse electrodialysis stacks by a validated model, J. Membr. Sci. 310 (2008) 418–430.
[21] P. Długołęcki, A. Gambier, A.K. Nijmeijer, M. Wessling, Practical potential of reverse electrodialysis as process for sustainable energy generation, Environ. Sci. Technol. 43 (2009) 6888–6894.
[22] P. Długołęcki, B. Anet, S.J. Metz, K. Nijmeijer, M. Wessling, Transport limitations in ion exchange membranes at low salt concentrations, J. Membr. Sci. 346 (2010) 163–171.
[23] P. Długołęcki, P. Ogonowski, S.J. Metz, K. Nijmeijer, M. Wessling, On the resistances of membrane, diffusion boundary layer and double layer in ion exchange membrane transport, J. Membr. Sci. 349 (2010) 369–379.
[24] P. Długołęcki, K. Nymeijer, S. Metz, M. Wessling, Current status of ion exchange membranes for power generation from salinity gradients, J. Membr. Sci. 319 (2008) 214–222.
[25] P. Długołęcki, J. Dąbrowska, K. Nijmeijer, M. Wessling, Ion conductive spacers for increased power generation in reverse electrodialysis, J. Membr. Sci. 347 (2010) 101–107.
[26] J.W. Post, C.H. Goeting, J. Valk, S. Goinga, J. Veerman, H.V.M. Hamelers, P.J.F.M. Hack, Towards implementation of reverse electrodialysis for power generation from salinity gradients, Desalination Water Treat. 16 (2010) 182–193.
[27] E. Brauns, Salinity gradient power by reverse electrodialysis: effect of model parameters on electrical power output, Desalination 237 (2009) 378–391.